Accepted Manuscript

Title: Autophagy-mediated neuroprotection induced by octreotide in an *ex vivo* model of early diabetic retinopathy

Authors: Rosario Amato, Elisabetta Catalani, Massimo Dal Monte, Maurizio Cammalleri, Ilaria Di Renzo, Cristiana Perrotta, Davide Cervia, Giovanni Casini

PII: S1043-6618(17)30985-4
DOI: https://doi.org/10.1016/j.phrs.2017.09.022
Reference: YPHRS 3697

To appear in: *Pharmacological Research*

Received date: 3-8-2017
Revised date: 21-9-2017
Accepted date: 28-9-2017

Please cite this article as: Amato Rosario, Catalani Elisabetta, Dal Monte Massimo, Cammalleri Maurizio, Di Renzo Ilaria, Perrotta Cristiana, Cervia Davide, Casini Giovanni.Autophagy-mediated neuroprotection induced by octreotide in an ex vivo model of early diabetic retinopathy.*Pharmacological Research* https://doi.org/10.1016/j.phrs.2017.09.022

This is a PDF file of an unedited manuscript that has been accepted for publication. As a service to our customers we are providing this early version of the manuscript. The manuscript will undergo copyediting, typesetting, and review of the resulting proof before it is published in its final form. Please note that during the production process errors may be discovered which could affect the content, and all legal disclaimers that apply to the journal pertain.

ACCEPTED MANUSCRIPT

Autophagy-mediated neuroprotection induced by octreotide in an *ex vivo* model of early diabetic retinopathy

Running title: Octreotide stimulates autophagy in high glucose-treated retinas

Rosario Amato[1], Elisabetta Catalani[2], Massimo Dal Monte[1,3], Maurizio Cammalleri[1], Ilaria Di Renzo[4], Cristiana Perrotta[4], Davide Cervia[2,*], Giovanni Casini[1,3,*]

[1]Department of Biology, University of Pisa, Pisa, Italy

[2]Department for Innovation in Biological, Agro-Food and Forest Systems (DIBAF), University of Tuscia, Viterbo, Italy

[3]Interdepartmental Research Center Nutrafood ‘‘Nutraceuticals and Food for Health’’, University of Pisa, Pisa, Italy

[4]Department of Biomedical and Clinical Sciences “Luigi Sacco” (DIBIC), University of Milano, Milano, Italy

*Corresponding authors:

Davide Cervia, PhD

Department for Innovation in Biological, Agro-food and Forest systems (DIBAF), University of Tuscia, largo dell’Università snc, Blocco D, 01100 Viterbo, Italy; d.cervia@unitus.it

Giovanni Casini, PhD

University of Pisa, Department of Biology, Unit of General Physiology, via S. Zeno 31, 56127 Pisa, Italy; giovanni.casini@unipi.it

ACCEPTED MANUSCRIPT

Graphical abstract

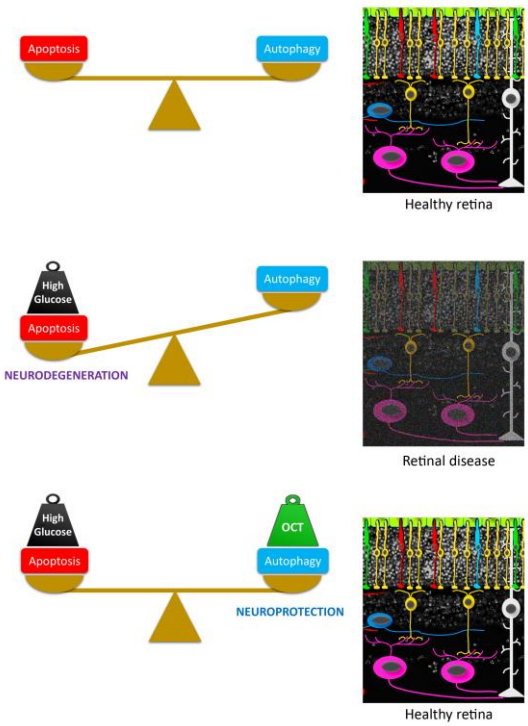

ABSTRACT

Neuronal injury plays a major role in diabetic retinopathy (DR). Our hypothesis was that the balance between neuronal death and survival may depend on a similar equilibrium between apoptosis and autophagy and that a neuroprotectant may act by influencing this equilibrium. *Ex vivo* mouse retinal explants were treated with high glucose (HG) for 10 days and the somatostatin analog octreotide (OCT) was used as a neuroprotectant. Chloroquine (CQ) was used as an autophagy inhibitor. Apoptotic and autophagic markers were evaluated using western blot and immunohistochemistry. HG-treated explants displayed a significant increase of apoptosis paralleled by a significant decrease of the autophagic flux, which was likely to be due to increased activity of the autophagy regulator mTOR (mammalian target of rapamycin). Treatment with OCT rescued HG-treated retinal explants from apoptosis and determined an increase of autophagic activity with concomitant mTOR

ACCEPTED MANUSCRIPT

inhibition. Blocking the autophagic flux with CQ completely abolished the anti-apoptotic effect of OCT. Immunohistochemical observations showed that OCT-induced autophagy is localized to populations of bipolar and amacrine cells and to ganglion cells. These observations revealed the antithetic role of apoptosis and autophagy, highlighting their equilibrium from which neuronal survival is likely to depend. These data suggest the crucial role covered by autophagy, which could be considered as a molecular target for DR neuroprotective treatment strategies.

Keywords: Autophagic flux, Apoptosis, Somatostatin, Bipolar cells, Amacrine cells, Ganglion cells.

1. Introduction

Diabetic retinopathy (DR) is a leading cause of blindness in the world. Because of its typical vascular dysfunctions and aberrant angiogenesis, this disease has long been considered exclusively as a microvascular disorder of the retina. However, that neuronal injury plays a major role in DR is gaining increasing recognition [1-4].

Apoptotic pathways are known to participate in the death of retinal cells under different noxious stimuli, including diabetic stress, but autophagy, a catabolic pathway that promotes the degradation and recycling of cellular components, has also been recognized to be involved in the fate of stressed retinal neurons [5, 6]. A variety of studies has been concerned with the possible roles of autophagy in DR [7-11]. Although the modulation of autophagic signaling, with consequent autophagy dysregulation, is likely to be involved in the pathogenesis of DR [11-13], whether high glucose (HG) levels determine an increase of the autophagic flux or, instead, inhibit autophagy, has not been established unambiguously. Indeed, in retinal pigment epithelial cells, HG has been observed to cause a marked increase in autophagy and autophagosome formation [14, 15], while in

ACCEPTED MANUSCRIPT

Müller cells HG has been observed to disrupt autophagy and induce cargo accumulation due to lysosomal dysfunction [13].

Another interesting point is whether we should expect pro-survival or pro-death effects of autophagy in DR [8, 11, 16]. Apoptosis and necrosis seem to establish a strict relationship with autophagy, which may function as a cell death route or may initiate a cell protective response [17]. For instance, in retinal pericytes under mild stress related to DR, autophagy may confer protection, while under more severe stress it could promote cell death [12]. Several observations seem to favor a cytoprotective role of autophagy in DR: in retinal pigment epithelial cells and in Müller cells the inhibition of autophagy increases HG-induced cell death [13, 15], while activation of autophagy protects cells from apoptosis [13]. In general, it is known that autophagy and apoptosis are under the control of common intracellular effectors, resulting in cross-regulation. Thus, autophagy would reduce the propensity of cells to undergo apoptosis, while apoptotic signaling, in turn, would inhibit autophagy [18, 19]. Although little is known of the balance between apoptosis and autophagy in retinal neurons during early phases of DR, a neuroprotective treatment may act by influencing this equilibrium. Indeed, there is clear evidence that neurons possess the machinery for autophagy, while an efficient autophagic function has been found to be positively associated with neuroprotection in different regions of the central nervous system [20-22], including the retina [6, 23].

Apoptosis of retinal neurons can be effectively inhibited with the somatostatin neuropeptide analog octreotide (OCT) [24-29]. In particular, our data show that protecting retinal neurons from diabetic stress also reduces the expression and release of vascular endothelial growth factor (VEGF), suggesting that neuroprotective agents may decrease the risk, in the long term, of pathologic angiogenesis [24]. Different roles of endogenous neuropeptides, including somatostatin, in the regulation of autophagy have been recently highlighted [30], which may provide a better knowledge of the molecular mechanisms and the functional dynamics of the autophagic process as well as its pathophysiology. Therefore, we investigated a possible involvement of autophagy in the

ACCEPTED MANUSCRIPT

neuroprotective effects exerted by OCT in our established *ex vivo* model of retinal explants cultured in HG [24].

2. Materials and Methods

2.1. Animals

The procedures were approved by the Ethics Committee in Animal Experiments of the University of Pisa (Pisa, Italy) and were in compliance with the ARVO Statement for the Use of Animals in Ophthalmic and Vision Research, the Italian guidelines for animal care (DL 116/92), and the EU Directive (2010/63/EU). All experimental procedures were performed to reduce both animal suffering and the number of animals used. C57BL/6J mice (Charles River Laboratories) were used in these studies. They were kept in a regulated environment (23 ± 1°C, 50 ± 5% humidity) with a 12-hour light/dark cycle (lights on at 8 AM) with food and water *ad libitum*.

2.2. Ex-vivo retinal explants

Retinas from 4- to 5-week-old mice of both sexes were dissected in Modified Eagle Medium (MEM; Sigma-Aldrich, St. Louis, MO, USA) and cut into 4 fragments. The fragments were transferred onto Millicell-CM culture inserts (Merck Millipore, Darmstadt, Germany) with ganglion cells up. The inserts were placed in 6-well tissue culture plates with 1 mL of serum-free culture medium composed of 50% MEM/HEPES (Sigma-Aldrich) containing 6 mM D-glucose, 25% Hank's buffer salt solution (Sigma-Aldrich), 25% PBS, 25 U/mL penicillin, 25 mg/mL streptomycin, 1 μg/mL amphotericin B, and 200 μM L-glutamine. The explants were incubated for 10 days at 37°C under a humidified 95%/5% (vol/vol) mixture of air and CO_2. The medium was changed every other day. The HG condition was realized by adding D-glucose to the culture medium to reach a concentration of 75 mM. As previously reported, although in different studies HG treatments have been performed using a wide variety of glucose concentrations, in our

ACCEPTED MANUSCRIPT

experimental model treatments with 75 mM glucose are necessary to induce significant increases of apoptotic markers [24].

Control experiments were performed using a culture medium containing 6 mM D-glucose and 69 mM mannitol. Consistent with our previous findings [24], the amount of apoptotic cell death in mannitol-treated explants, evaluated with western blot for cleaved caspase-3, was not significantly different from that in untreated explants (not shown). These observations were also in agreement with previous studies of rat retinal explants [31]. Based on these findings, untreated explants were used as controls.

2.3. Pharmacologic treatments

The somatostatin analogue octreotide (OCT, Sigma-Aldrich), a long-lasting agonist at the somatostatin subtype 2 (sst_2) receptor [32-36], was used at 1 µM concentration according to our previous work [24]. Chloroquine (CQ, Sigma-Aldrich) is a lysosomotropic agent that prevents acidification of the lysosomal lumen and inhibits the activity of lysosomal enzymes [37]. It was used as an inhibitor of the autophagic flux at a concentration of 10 µM, according to the literature [38, 39].

2.4. Western blot

At the end of the incubation period, each retinal fragment was collected and lysed in 50 µL of 10 mM Tris/HCl, pH 7.6, containing 5 mM EDTA, 3 mM EGTA, 250 mM sucrose, and 1% SDS, and supplemented with a cocktail of protease and phosphatase inhibitors. Equal amounts of proteins were separated by 4-20% SDS-polyacrylamide gel electrophoresis and transferred onto nitrocellulose membrane using a Bio-Rad Trans-Blot Turbo System. The membranes were then probed using primary antibodies and directed to microtubule-associated protein light chain 3 (LC3)

ACCEPTED MANUSCRIPT

(Cell Signaling Technology, Danvers, MA, USA, #4108), to p62 (Sigma-Aldrich, #P0068), to S6 Ribosomal Protein phosphate (pS6) (Cell Signaling Technology, #2215), or to cleaved caspase-3 (Cell Signaling Technology, #9664). After incubation with the appropriate horseradish-peroxidase-conjugated secondary antibody, immunoreactive bands were visualized using the Clarity Western ECL substrate with a ChemiDoc XP imaging system (Bio-Rad Laboratories, Segrate, Milano, Italy). Bands were quantified for densitometry using the Image Lab software (Bio-Rad Laboratories) and normalized to GAPDH (Santa Cruz Biotechnology, Dallas, TX, USA, #sc-25778).When appropriate, the primary antibody that recognises the protein independently of its phosphorylation state, *i.e.* S6 ribosomal protein (Cell Signaling Technology, #2317), was also used in reprobing experiments for normalization purposes.

2.5. Immunofluorescence

Retinal fragments were fixed in 4% paraformaldehyde in 0.1M phosphate buffer (PB) for 1 h. They were stored overnight in 25% sucrose in PB and subsequently embedded in cryo-gel and frozen using liquid nitrogen. Sections (10 μm thick) were cut on a cryostat, mounted onto gelatinized slides and stored at -20°C until use. For immunostaining, sections were washed in PB and pre-incubated for 15 min at room temperature with 5% bovine serum albumin (BSA; Life Technologies) and 10% of normal goat serum (Life Technologies, Monza, Italy) in PB containing 0.5% Triton X-100. The slides were then incubated overnight at 4°C with primary antibodies directed to LC3 (Sigma-Aldrich, #L8918; dilution 1:100), to p62 (Sigma-Aldrich, #P0067, dilution 1:200) or to cleaved caspase-3 (Sigma-Aldrich, #C8487; dilution 1:400) diluted in PB containing 0.5% Triton X-100.

In double-label immunofluorescence experiments, the LC3 antibody was used in conjunction with antibodies directed to MAb115A10 (from Dr. S.C. Fujita, of the Mitsubishi Kasei Institute of Life Sciences, Tokyo, Japan; dilution 1:1000), gamma-aminobutyric acid transporter-1

ACCEPTED MANUSCRIPT

(GAT-1, Merck Millipore, #AB1570; dilution 1:200), Disabled-1 (Dab1, Sigma Aldrich, #SAB4503448; dilution 1:300) , or ß tubulin III (Sigma Aldrich, #T8660; dilution 1:400).

The double labeling experiments with LC3 antibodies in conjunction with antibodies directed to GAT-1 or to Dab1, which are all made in rabbit, were performed following published protocols [40]. Briefly, sections were first incubated with the primary antibody directed to LC3 for 3 h at room temperature and then in anti-rabbit fluorescein-conjugated Fab fragment antibody (Jackson Immuno Research, Suffolk, UK, #JI111097003) for 1.5 h at room temperature. Subsequently, the slides were incubated in anti-rabbit unlabeled Fab fragment antibody (Jackson Immuno Research, # JI111007003) overnight at 4°C and then, after washes in PB, with the antibody directed to GAT-1 or to Dab1 for 3 h at room temperature. Following washes in PB, the sections were incubated with secondary anti-rabbit antibodies conjugated with Alexa-Fluor-546 (Life Technologies) at a dilution of 1:400 in PB containing 0.5% Triton X-100, for 1.5 h at room temperature.

The slides were coverslipped with Fluoroshield Mounting Medium containing DAPI (Abcam, Cambridge, UK). Images were acquired using a Zeiss Axioskop 2 plus microscope equipped with the Axiocam MRC photocamera and the Axiovision software (Carl Zeiss, Oberkochen, Germany) or a Zeiss LSM 710 confocal microscope (Carl Zeiss). Final images were sized and optimized for contrast and brightness using Adobe Photoshop (Adobe Systems, Mountain View, CA, USA). The images of double-label immunofluorescence were checked for how they are perceived by the colorblind [41].

To perform quantitative analysis in LC3 immunostained retinas, at least five representative images acquired with the Zeiss Axioscop were selected for each retinal explant and four explants, each originating from a different retina, for experimental condition were analyzed. Each image was converted to grayscale and normalized to background using an image editing software (Adobe Photoshop). Mean gray levels were then measured in the area encompassing the ganglion cell layer

ACCEPTED MANUSCRIPT

(GCL), the inner plexiform layer (IPL), the inner nuclear layer (INL), and the outer plexiform layer (OPL).

2.6. Statistics

Statistical significance of data between the groups was evaluated using unpaired Student's t-test (single comparisons) and one-way ANOVA (multiple comparisons) followed by the Tukey's or Newman-Keuls post-tests. The results were expressed as means ± SEM. Prism 5 (GraphPad Software, Inc., La Jolla, CA, USA) was used to analyze the data. Differences with $p < 0.05$ were considered statistically significant.

3. Results

3.1 Autophagy in HG-treated explants and effects of OCT

LC3 is an ubiquitin-like protein that may be found in an unconjugated, slow migrating form (LC3-I) or conjugated to the membranes of autophagic vesicles in a lipidated, fast migrating form (LC3-II) [42]. An increase in the expression of LC3-II reflects an increase of autophagosomes in the cells. As shown in figure 1A, HG reduced LC3-II levels to about one-half of those in control explants, while OCT treatment resulted in a dramatic increase of LC3-II indicating a remarkable accumulation of autophagic vesicles induced by the neuroprotectant. Since the lipidation of LC3 may be the result of both induction and suppression of autolysosomal maturation, the measurement of p62, a cargo receptor for the autophagic degradation of ubiquitinated substrates that is degraded during autophagy [43], is a useful method to distinguish whether autophagosome accumulation is due to autophagy induction or rather to the inhibition of autophagy steps [42]. As shown in figure

ACCEPTED MANUSCRIPT

1B, p62 levels were significantly increased in HG-treated explants, but they were not significantly different from control values in HG-treated explants incubated in the presence of OCT. Together, these data indicated that HG induced a decrease of autophagy, which was restored by the treatment with OCT.

The regulation of autophagy involves a complex machinery, in which the main autophagy regulator is mammalian (or mechanistic) target of rapamycin (mTOR). An increase of mTOR activity inhibits, while a decrease of mTOR activity promotes, the autophagic flux [44]. To assess the involvement of mTOR in our experimental model, we evaluated the phosphorylation rate of protein S6. This protein is phosphorylated as a consequence of mTOR activation [44], therefore the level of pS6 is commonly considered as a marker of mTOR activity [42]. Figure 1C shows that the ratio pS6/S6 was significantly increased in HG-treated explants, but it came back to control values in the presence of OCT, indicating that the changes in autophagic function observed in HG-treated explants with or without OCT are coupled to mTOR.

3.2. Expression patterns of autophagic markers

Changes in autophagic function could also be appreciated with immunohistochemistry. LC3 immunofluorescence was detected in control, untreated explants (Fig. 2A), where LC3 immunoreactivity was mainly localized to the OPL and to the GCL, with some sparse LC3 immunostained puncta that could be also seen in the distal INL. Although in most explants the general picture was similar to that represented in figure 2A, in some cases only the OPL or the GCL immunolabeling could be observed. The LC3 immunostaining was mostly diffuse, with scattered aggregates (Fig. 2A, insets). In HG-treated explants, LC3 immunolabeling was dramatically reduced and only faint profiles could be observed in OPL and GCL (Fig. 2B), where immunostained puncta were barely visible (Fig. 2B, insets). When HG-treated explants were incubated in the presence of OCT, they displayed an intense LC3 immunostaining. The immunofluorescence in the OPL was relatively scarce and it was localized mainly to the INL and to

ACCEPTED MANUSCRIPT

the GCL, with scattered immunofluorescent puncta also visible in the IPL (Fig. 2C). LC3 immunostaining in the INL and GCL was characterized by strongly fluorescent aggregates (Fig. 2C, insets), which were particularly densely packed within the immunostained profiles in the GCL. The punctate appearance of LC3 immunolabeling was likely to be due to its presence in accumulating autophagosomes awaiting lysosomal degradation. A quantitative analysis of LC3 immunofluorescence intensity observed in the different experimental conditions (Fig. 2D) confirmed a significant decrease of LC3 expression caused by HG and the increased values in the presence of OCT.

Consistent with the western blot data, the immunostaining patterns of p62 showed a marked increase of p62 in the presence of HG, which was reverted by OCT treatment. In particular, p62 immunofluorescence was mostly localized to a few cells of the GCL in control explants (Fig. 3A) and in HG-treated explants in the presence of OCT (Fig. 3C). In contrast, explants incubated in HG alone displayed a widespread p62 immunofluorescence localized not only to the GCL, but also to the mid- and distal INL, where immunofluorescent profiles were characterized by strongly immunolabeled puncta (Fig. 3B).

Double-label immunofluorescence was performed to gather some information about the cellular types expressing autophagy markers. To this aim, the antibody directed to LC3 was used in conjunction with other antibodies for the visualization of populations of bipolar cells, amacrine cells, and ganglion cells in explants treated with both HG and OCT. The MAb115A10 antibody recognizes an antigen expressed by rod and ON-type cone bipolar cells in the mouse retina [45]. As shown in figure 4A-C, the intensely immunolabeled LC3 puncta in the distal INL were not within MAb115A10 immunoreactive profiles, therefore ON-type bipolar cells did not appear to be the main site of autophagy regulation in the INL. However, a closer observation revealed that these bipolar cells contained a number of LC3 puncta showing dimmer immunostaining (Fig. 4C, inset), indicating that they may participate to autophagic mechanisms, although to a lesser extent. Regarding amacrine cells expressing LC3 immunoreactivity, double immunolabeling was

ACCEPTED MANUSCRIPT

performed using an antibody directed to GAT-1, which identifies the majority of GABAergic amacrine cells [46]. Only a few LC3 immunostained cells also displayed GAT-1 immunoreactivity on their membrane (Fig. 4D-F), indicating that the most of LC3 expressing amacrine cells were not GABAergic. In particular, immunolabeled cell counting in double labeled retinal sections indicated that the numbers of GAT-1 immunolabeled cells was similar to that of LC3 immunoreactive cells located in the proximal INL and that about 20% of them were double labeled. The presence of LC3 immunoreactivity was also investigated in the glycinergic AII amacrine cells, identified with antibodies directed to Dab1 [47]. As shown in figure 4 G-I, many double-labeled profiles were observed in the proximal INL, indicating that the vast majority of LC3 immunostained cells were, in fact, glycinergic, AII amacrine cells. To evaluate the presence of LC3 puncta in ganglion cells, double label experiments were performed using an antibody directed to ß-tubulin III, which is expressed by ganglion cells [48]. As sown in figure 4J-L, virtually all LC3 immunostained profiles in the GCL were also ß-tubulin III immunolabeled, and vice-versa, indicating a central involvement of ganglion cells in autophagic modulation that may occur in DR.

3.3. Effects of OCT on the autophagic flux in HG-treated retinas

To investigate in more detail the effects of OCT on the autophagic machine, a set of experiments was conducted in the presence of CQ, an inhibitor of autophagy. In particular, CQ blocks lysosome acidification, thereby preventing its fusion with the autophagosome and inhibiting autophagosome degradation [49]. Thus, the extent of LC3 turnover in response to CQ reflects the rate of autophagic degradation, or autophagic flux [42]. To demonstrate that OCT was in fact enhancing the autophagic flux, we evaluated the LC3-II levels in the absence and in the presence of CQ. As shown in Fig. 5A, CQ treatment induced a significant increase of LC3-II levels in the explants treated with HG and an even greater increase in the explants treated with both HG and OCT. The analysis of the data by the LC3-II turnover assay [50] revealed that OCT significantly increased the LC3-II net flux in HG-treated retinal explants (Fig. 5B).

ACCEPTED MANUSCRIPT

Consistent with these observations, in immunofluorescence experiments HG-treated explants incubated in the presence of CQ or of both OCT and CQ, displayed a LC3 immunofluorescence that was enhanced with respect to that in explants incubated with HG alone and that was extensively localized to the OPL, INL, IPL, and GCL (Fig. 6A-C). In the explants incubated in the presence of CQ, the LC3 immunoreactive profiles were characterized by large, brightly fluorescent puncta (Fig. 6A-C, insets). A quantitative evaluation of the immunofluorescence intensity confirmed the data obtained with the western blots (Fig. 6D). In summary, the increases of LC3-II turnover, LC3-II net flux, and LC3-II aggregates in HG-treated retinas indicated that the CQ-induced blockade of the autophagic flux determined an accumulation of undegraded autophagosomes expressing LC3-II immunoreactivity and that OCT acts stimulating the autophagic flux.

3.4. Effects of autophagy blockade on OCT antiapoptotic action

To investigate the relationship between autophagy and apoptosis in HG-treated retinal explants and to evaluate the possible involvement of autophagy in the protective effects exerted by OCT, we evaluated the expression of cleaved (active) caspase-3 as a marker of apoptosis. As expected [24], apoptosis was increased in HG-treated explants and was reduced below control levels in explants treated with both HG and OCT (Fig. 7). Interestingly, in all the experimental conditions (untreated control, HG-treated, and HG-treated plus OCT), the administration of CQ provoked a marked increase of active caspase-3 levels. In particular, the protective effect of OCT in HG-treated explants was abolished by CQ.

To better visualize the relationship between autophagy and apoptosis, LC3 and active caspase-3 immunostainings were compared in retinal sections from of control, HG-treated, and HG plus OCT-treated retinal explants. As shown in figure 10, in control explants basal LC3 immunoreactivity corresponded to the presence of scarce apoptotic profiles (Fig. 8A-C); in HG-treated explants, only faint LC3 immunostaining could be observed, and it was paralleled by an increase of active

ACCEPTED MANUSCRIPT

caspase-3 immunostained cells (Fig. 8D-F); in HG-treated explants incubated in the presence of OCT, the appearance of strong LC3 immunoreactivity characterized by brightly immunofluorescent puncta corresponded to a pattern of active caspase-3 immunostaining that was similar to that observed in control explants (Fig. 8G-I).

Together, these results indicated that the inhibition of autophagy caused cell death and, of interest, that OCT stimulation of the autophagic flux protected retinal neurons from HG-induced apoptosis.

4. Discussion

We have demonstrated recently that, in an *ex vivo* model of early DR, OCT is very effective in reducing both apoptosis and VEGF expression and release. In particular, our data indicated that VEGF levels directly depend on the efficacy of neuroprotection [24]. Therefore, both neural and vascular damages in DR may be prevented using neuroprotective substances in early phases of the disease [4] and the mechanisms mediating the neuroprotective properties of substances like OCT deserve attention. Here, we provide data supporting a central role of autophagy in such mechanisms.

4.1. Autophagy and retinal disease

Autophagic mechanisms are likely to be involved in the pathogenesis of different ocular diseases other than DR [9]. For example, a reduction of autophagosomes and autophagic flux has been reported both in retinas of mouse models of age-related macular degeneration (AMD) and in ocular tissues of AMD patients [51], suggesting that, in the presence of dysregulated autophagy, constant oxidative stress, increased protein aggregation, and inflammation may cause the pathological phenotype of AMD [52]. In addition, in a mouse model of retinitis pigmentosa, blockade of the autophagic flux has been found to be associated to photoreceptor degeneration [53]. Autophagy is also involved in glaucoma; although its effects in retinal ganglion cells and in their

ACCEPTED MANUSCRIPT

axons are not always easy to resolve, autophagy is likely to mainly exert protective actions in this disease [54]. In general, our observations are consistent with these findings and with the view that autophagy plays a pro-survival role in the retina under noxious stimuli; however, there are also reports indicating that induction of autophagy may lead to the death of retinal neurons. Indeed, an increase of autophagic markers has been found to be associated to ganglion cell death induced by ischemia/reperfusion in rats [55] or to rod photoreceptor death in streptozotocin-treated, diabetic mice [56].

4.2. Autophagy and OCT-mediated neuroprotection in DR

Our data demonstrate that, in *ex vivo* retinal explants, the stress induced by HG disrupts autophagy, leading to apoptotic cell death of retinal neurons, and that this decreased autophagy is associated with an up-regulation of mTOR activity. These observations are consistent with a nutrient regulation of mTOR induced by HG. Indeed, in nutrient-rich conditions, such as HG, mTOR is known to be activated and to promote synthetic activities and cell growth, while in nutrient-deficient conditions mTOR is inhibited and catabolic processes are activated to produce sufficient energy for survival [57]. This nutrient regulation of mTOR is likely to have an impact on the autophagic flux and on apoptotic levels in different circumstances. For instance, it has been reported that, in the mouse hippocampus, caloric restriction inhibits mTOR expression and function leading to increased autophagy, which results in neuroprotection [58, 59].

The multiple roles that peptides may play in the regulation of autophagy have been reviewed recently [30]. The somatostatin analog OCT is known to exert powerful neuroprotective actions in the retina [24-29, 60]. Our results show that the administration of this neuroprotectant to HG-treated retinal explants inhibits mTOR and re-activates the autophagy machine thus increasing the autophagic flux. This positive effect of OCT on autophagy is coupled to the OCT well-known anti-apoptotic actions, since our results demonstrate that the anti-apoptotic efficacy of OCT is completely abolished when the autophagic flux is blocked by CQ. Interestingly, OCT has been

ACCEPTED MANUSCRIPT

recently found to exert protective effects in the kidney after hepatic ischemia through induction of autophagy [61]. A wide variety of data support the notion that autophagy plays a fundamental role in preventing neurodegeneration [22, 62, 63], and perturbations of autophagy are thought to participate to the pathogenesis of all major neurodegenerative diseases [64, 65]. In our model of early DR, the neuroprotection afforded by OCT is mediated by the OCT-promoted activation of the autophagic flux.

Interestingly, in the same experimental model of the present study we have observed recently that the neuroprotective effect OCT also results in inhibition of VEGF expression and release [24]. If the protective effect of OCT is mediated by mTOR inhibition and increased autophagy, the possibility exists that OCT may induce VEGF inhibition through the same pathway. In effect, it has been reported that blocking mTOR with rapamycin reduces VEGF expression in the retinas of streptozotocin-treated rats with DR [66] and VEGF release in cultured Müller cells in the presence of HG [13]. In addition, in retinal pigment epithelial cells, activation of mTOR has been found to be important for VEGF expression [67], while VEGF expression and/or release are reduced in the presence of mTOR inhibition obtained with rapamycin [68-70] or with other drugs [71-73].

Autophagy activation by OCT has been visualized within retinal layers using immunohistochemistry. In line with previous reports, LC3 immunoreactivity was localized to the OPL, INL, IPL, and GCL [56, 74]. In particular, LC3 immunoreactivity in HG-treated explants in the presence of OCT is significantly increased with respect to HG-treated explants without OCT, and it shows a pattern characterized by a number of cells in both the GCL and the INL containing many brightly immunofluorescent puncta. These observations, and in particular the appearance of the LC3 immunofluorescent puncta, indicate an increase of autophagosome formation induced by OCT.

4.3. Retinal neuronal populations involved in the OCT-induced increase of autophagy

ACCEPTED MANUSCRIPT

Our results show that, in HG-treated retinal explants, OCT induces an increase of LC3 immunolabeled puncta in different neuronal types of the retina. In particular, ON-type bipolar cells (which include ON-cone bipolar cells and rod bipolar cells) appear to increase their LC3 expression in the presence of OCT, at least to a certain extent. However, the most intensely LC3 immunolabeled profiles do not belong to these bipolar cells. Based on their localization in the mid-distal INL, they are likely to belong to other bipolar cells, which can be classified as OFF-type bipolar cells. In summary, in the presence of a stress caused by HG, the treatment with OCT induces an increase of LC3 puncta (indicating increased autophagy) in most, if not all, bipolar cells, especially the OFF-type. In addition to bipolar cells, virtually all ganglion cells also display bright LC3 puncta. Our previous studies showed that OCT is capable of protecting *ex vivo* mouse retinas from acute ischemic insults by inhibiting excessive glutamate release caused by ischemia [27, 28]. Since glutamate excitotoxicity is likely to play a role in the neuronal damage caused by HG [4], it is interesting to note that OCT-induced autophagy, mapped with LC3 immunofluorescence, is mainly localized to OFF bipolar and ganglion cells, which are known to be glutamatergic and to express ionotropic glutamate receptors [75].

A number of LC3 immunostained cells localize to the proximal INL, and therefore these cells are likely to be amacrine cells. We did not test the presence of LC3 in dopaminergic amacrine cells because these cells represent only a very sparse population in the retina. In addition, the classic localization pattern of cholinergic amacrine cells (two mirror-symmetric populations in the proximal INL and in the GCL) was not consistent with the observed localization of LC3 immunostaining, and therefore double label experiments with LC3 together with a cholinergic marker were not performed. The number of LC3 immunostained amacrine cells results to be similar to that of GABAergic amacrine cells, indicating that a relatively high number of amacrine cells is involved in OCT-induced autophagic regulation. Regarding the type of amacrine cells that these cells may represent, our data show that only a small percentage of them are likely to be GABAergic. Since all amacrine cells in vertebrate retinas can be accounted for by the two

ACCEPTED MANUSCRIPT

inhibitory neurotransmitters GABA and glycine [76], it follows that the majority of amacrine cells with OCT-induced LC3 immunoreactivity are glycinergic amacrine cells. In particular, the double label experiments with Dab1 indicate that these cells belong to the population of AII amacrine cells.

In summary, an analysis of the neuronal populations in which, in the presence of a diabetic stress, OCT induces an increase of the autophagic flux suggests that autophagy may help glutamatergic neurons to re-equilibrate glutamate release and glutamate receptor-expressing neurons to resist to glutamate-driven excitation.

5. Conclusion

The data presented here indicate that a cross talk between apoptosis and autophagy is likely to exist in the retina. It may be altered by stressing conditions favoring apoptosis, but it may be re-equilibrated by autophagy-stimulating substances. In particular, our results indicate that the reported antiapoptotic actions of OCT are the result of a stimulation of the autophagic flux. These observations support the possibility of targeting autophagic mechanisms for interventions in the early phases of DR.

Source of funding

This work was supported by grants from the “Ministero dell’Istruzione, Università e Ricerca” (PRIN2015) and from the University of Pisa (PRA-2016).

Conflicts of interest

None.

Acknowledgments

ACCEPTED MANUSCRIPT

The authors wish to thank Gino Bertolini and Dr. Angelo Gazzano (University of Pisa, Italy) for assistance with the mouse colonies.

ACCEPTED MANUSCRIPT

References

1. A.J. Barber, A new view of diabetic retinopathy: a neurodegenerative disease of the eye, Progress in Neuro-Psychopharmacology & Biological Psychiatry 27 (2003) 283-290.
2. V. Jindal, Neurodegeneration as a Primary Change and Role of Neuroprotection in Diabetic Retinopathy, Molecular Neurobiology 51 (2015) 878-884.
3. X.Y. Zhang, N.L. Wang, G.R. Barile, S.S. Bao, M. Gillies, Diabetic retinopathy: Neuron protection as a therapeutic target, International Journal of Biochemistry & Cell Biology 45 (2013) 1525-1529.
4. C. Hernandez, M. Dal Monte, R. Simo, G. Casini, Neuroprotection as a Therapeutic Target for Diabetic Retinopathy, J Diabetes Res 2016 (2016) 9508541.
5. N.D. Chinskey, C.G. Besirli, D.N. Zacks, Retinal cell death and current strategies in retinal neuroprotection, Curr Opin Ophthalmol 25 (2014) 228-233.
6. R. Russo, L. Berliocchi, A. Adornetto, D. Amantea, C. Nucci, C. Tassorelli, L.A. Morrone, et al., In search of new targets for retinal neuroprotection: is there a role for autophagy?, Curr Opin Pharmacol 13 (2013) 72-77.
7. P. Boya, L. Esteban-Martinez, A. Serrano-Puebla, R. Gomez-Sintes, B. Villarejo-Zori, Autophagy in the eye: Development, degeneration, and aging, Prog Retin Eye Res 55 (2016) 206-245.
8. P. Chai, H. Ni, H. Zhang, X. Fan, The Evolving Functions of Autophagy in Ocular Health: A Double-edged Sword, Int J Biol Sci 12 (2016) 1332-1340.
9. Y.J. Li, Q. Jiang, G.F. Cao, J. Yao, B. Yan, Repertoires of autophagy in the pathogenesis of ocular diseases, Cell Physiol Biochem 35 (2015) 1663-1676.
10. J.H. Ma, J.J. Wang, S.X. Zhang, The unfolded protein response and diabetic retinopathy, J Diabetes Res 160140 (2014) 29.
11. M.D. Rosa, G. Distefano, C. Gagliano, D. Rusciano, L. Malaguarnera, Autophagy in Diabetic Retinopathy, Curr Neuropharmacol 14 (2016) 810-825.
12. D. Fu, J.Y. Yu, S. Yang, M. Wu, S.M. Hammad, A.R. Connell, M. Du, et al., Survival or death: a dual role for autophagy in stress-induced pericyte loss in diabetic retinopathy, Diabetologia 59 (2016) 2251-2261.
13. J.M. Lopes de Faria, D.A. Duarte, C. Montemurro, A. Papadimitriou, S.R. Consonni, J.B. Lopes de Faria, Defective Autophagy in Diabetic Retinopathy, Invest Ophthalmol Vis Sci 57 (2016) 4356-4366.
14. J. Yao, Z.F. Tao, C.P. Li, X.M. Li, G.F. Cao, Q. Jiang, B. Yan, Regulation of autophagy by high glucose in human retinal pigment epithelium, Cell Physiol Biochem 33 (2014) 107-116.
15. H. Shi, Z. Zhang, X. Wang, R. Li, W. Hou, W. Bi, X. Zhang, Inhibition of autophagy induces IL-1β release from ARPE-19 cells via ROS mediated NLRP3 inflammasome activation under high glucose stress, Biochemical and Biophysical Research Communications 463 (2015) 1071-1076.
16. L.S. Frost, C.H. Mitchell, K. Boesze-Battaglia, Autophagy in the eye: implications for ocular cell health, Exp Eye Res 124 (2014) 56-66.
17. C. Swart, A. Du Toit, B. Loos, Autophagy and the invisible line between life and death, Eur J Cell Biol 95 (2016) 598-610.
18. C. Gordy, Y.W. He, The crosstalk between autophagy and apoptosis: where does this lead?, Protein Cell 3 (2012) 17-27.
19. Y. Maejima, S. Kyoi, P. Zhai, T. Liu, H. Li, A. Ivessa, S. Sciarretta, et al., Mst1 inhibits autophagy by promoting the interaction between Beclin1 and Bcl-2, Nat Med 19 (2013) 1478-1488.

ACCEPTED MANUSCRIPT

20. L. Galluzzi, J.M. Bravo-San Pedro, K. Blomgren, G. Kroemer, Autophagy in acute brain injury, Nat Rev Neurosci 17 (2016) 467-484.
21. A.K. Singh, M.P. Kashyap, V.K. Tripathi, S. Singh, G. Garg, S.I. Rizvi, Neuroprotection Through Rapamycin-Induced Activation of Autophagy and PI3K/Akt1/mTOR/CREB Signaling Against Amyloid-beta-Induced Oxidative Stress, Synaptic/Neurotransmission Dysfunction, and Neurodegeneration in Adult Rats, Mol Neurobiol 22 (2016) 22.
22. Z.Y. Wang, J.Y. Liu, C.B. Yang, S. Malampati, Y.Y. Huang, M.X. Li, M. Li, et al., Neuroprotective Natural Products for the Treatment of Parkinson's Disease by Targeting the Autophagy-Lysosome Pathway: A Systematic Review, Phytother Res 15 (2017)
23. B. Fan, Y.J. Sun, S.Y. Liu, L. Che, G.Y. Li, Neuroprotective Strategy in Retinal Degeneration: Suppressing ER Stress-Induced Cell Death via Inhibition of the mTOR Signal, Int J Mol Sci 18 (2017)
24. R. Amato, M. Biagioni, M. Cammalleri, M. Dal Monte, G. Casini, VEGF as a Survival Factor in Ex Vivo Models of Early Diabetic Retinopathy, Invest Ophthalmol Vis Sci 57 (2016) 3066-3076.
25. U. Celiker, N. Ilhan, I. Ozercan, T. Demir, H. Celiker, Octreotide reduces ischaemia-reperfusion injury in the retina, Acta Ophthalmol Scand 80 (2002) 395-400.
26. D. Cervia, E. Catalani, M. Dal Monte, G. Casini, Vascular endothelial growth factor in the ischemic retina and its regulation by somatostatin, J Neurochem 120 (2012) 818-829.
27. D. Cervia, D. Martini, C. Ristori, E. Catalani, A.M. Timperio, P. Bagnoli, G. Casini, Modulation of the neuronal response to ischaemia by somatostatin analogues in wild-type and knock-out mouse retinas, J Neurochem 106 (2008) 2224-2235.
28. A. D'Alessandro, D. Cervia, E. Catalani, F. Gevi, L. Zolla, G. Casini, Protective effects of the neuropeptides PACAP, substance P and the somatostatin analogue octreotide in retinal ischemia: a metabolomic analysis, Mol Biosyst 10 (2014) 1290-1304.
29. J. Wang, Z. Sun, J. Shen, D. Wu, F. Liu, R. Yang, S. Ji, et al., Octreotide Protects the Mouse Retina against Ischemic Reperfusion Injury through Regulation of Antioxidation and Activation of NF-kappaB, Oxid Med Cell Longev 970156 (2015) 14.
30. E. Catalani, C. De Palma, C. Perrotta, D. Cervia, Current Evidence for a Role of Neuropeptides in the Regulation of Autophagy, Biomed Res Int 5856071 (2017) 16.
31. T. Oshitari, G. Bikbova, S. Yamamoto, Increased expression of phosphorylated c-Jun and phosphorylated c-Jun N-terminal kinase associated with neuronal cell death in diabetic and high glucose exposed rat retinas, Brain Res Bull 101 (2014) 18-25.
32. D. Cervia, D. Fehlmann, D. Hoyer, Native somatostatin sst2 and sst5 receptors functionally coupled to Gi/o-protein, but not to the serum response element in AtT-20 mouse tumour corticotrophs, Naunyn Schmiedebergs Arch Pharmacol 367 (2003) 578-587.
33. D. Cervia, S. Fiorini, B. Pavan, C. Biondi, P. Bagnoli, Somatostatin (SRIF) modulates distinct signaling pathways in rat pituitary tumor cells; negative coupling of SRIF receptor subtypes 1 and 2 to arachidonic acid release, Naunyn Schmiedebergs Arch Pharmacol 365 (2002) 200-209.
34. D. Cervia, P. Bagnoli, An update on somatostatin receptor signaling in native systems and new insights on their pathophysiology, Pharmacol Ther 116 (2007) 322-341.
35. D. Cervia, D. Langenegger, E. Schuepbach, M. Cammalleri, P. Schoeffter, H.A. Schmid, P. Bagnoli, et al., Binding and functional properties of the novel somatostatin analogue KE 108 at native mouse somatostatin receptors, Neuropharmacology 48 (2005) 881-893.
36. C. Nunn, D. Cervia, D. Langenegger, L. Tenaillon, R. Bouhelal, D. Hoyer, Comparison of functional profiles at human recombinant somatostatin sst2 receptor: simultaneous determination of intracellular Ca2+ and luciferase expression in CHO-K1 cells, Br J Pharmacol 142 (2004) 150-160.
37. C. Wang, Q. Hu, H.M. Shen, Pharmacological inhibitors of autophagy as novel cancer therapeutic agents, Pharmacol Res 105 (2016) 164-175.

ACCEPTED MANUSCRIPT

38. Y.C. Chang, M.C. Hsieh, H.J. Wu, W.C. Wu, Y.H. Kao, Methylglyoxal, a reactive glucose metabolite, enhances autophagy flux and suppresses proliferation of human retinal pigment epithelial ARPE-19 cells, Toxicol In Vitro 29 (2015) 1358-1368.
39. Y.H. Yoon, K.S. Cho, J.J. Hwang, S.J. Lee, J.A. Choi, J.Y. Koh, Induction of lysosomal dilatation, arrested autophagy, and cell death by chloroquine in cultured ARPE-19 cells, Invest Ophthalmol Vis Sci 51 (2010) 6030-6037.
40. E. Catalani, S. Tomassini, M. Dal Monte, L. Bosco, G. Casini, Localization patterns of fibroblast growth factor 1 and its receptors FGFR1 and FGFR2 in postnatal mouse retina, Cell Tissue Res 336 (2009) 423-438.
41. R. Roskoski, Jr. Guidelines for preparing color figures for everyone including the colorblind, Pharmacol Res. 2017 May;119:240-241. doi: 10.1016/j.phrs.2017.02.005. Epub 2017 Feb 8.
42. D.J. Klionsky, K. Abdelmohsen, A. Abe, M.J. Abedin, H. Abeliovich, A. Acevedo Arozena, H. Adachi, et al., Guidelines for the use and interpretation of assays for monitoring autophagy (3rd edition), Autophagy 12 (2016) 1-222.
43. M. Komatsu, S. Kageyama, Y. Ichimura, p62/SQSTM1/A170: physiology and pathology, Pharmacol Res 66 (2012) 457-462.
44. R.A. Saxton, D.M. Sabatini, mTOR Signaling in Growth, Metabolism, and Disease, Cell 168 (2017) 960-976.
45. S. Haverkamp, H. Wassle, Immunocytochemical analysis of the mouse retina, J Comp Neurol 424 (2000) 1-23.
46. G. Casini. Localization and Function of Gamma Aminobutyric Acid Transporter 1 in the Retina. In J. Tombran-Tinkand C.J. Barnstable (eds.), Ocular Transporters In Ophthalmic Diseases And Drug Delivery: Ophthalmology Research, Humana Press, Totowa, NJ, 2008, pp. 293-313.
47. D.S. Rice, T. Curran, Disabled-1 is expressed in type AII amacrine cells in the mouse retina, J Comp Neurol 424 (2000) 327-338.
48. M. Watanabe, U. Rutishauser, J. Silver, Formation of the retinal ganglion cell and optic fiber layers, J Neurobiol 22 (1991) 85-96.
49. H. Vakifahmetoglu-Norberg, H.G. Xia, J. Yuan, Pharmacologic agents targeting autophagy, J Clin Invest 125 (2015) 5-13.
50. N. Mizushima, T. Yoshimori, B. Levine, Methods in mammalian autophagy research, Cell 140 (2010) 313-326.
51. S.K. Mitter, C. Song, X. Qi, H. Mao, H. Rao, D. Akin, A. Lewin, et al., Dysregulated autophagy in the RPE is associated with increased susceptibility to oxidative stress and AMD, Autophagy 10 (2014) 1989-2005.
52. K. Kaarniranta, D. Sinha, J. Blasiak, A. Kauppinen, Z. Vereb, A. Salminen, M.E. Boulton, et al., Autophagy and heterophagy dysregulation leads to retinal pigment epithelium dysfunction and development of age-related macular degeneration, Autophagy 9 (2013) 973-984.
53. N. Rodriguez-Muela, A.M. Hernandez-Pinto, A. Serrano-Puebla, L. Garcia-Ledo, S.H. Latorre, E.J. de la Rosa, P. Boya, Lysosomal membrane permeabilization and autophagy blockade contribute to photoreceptor cell death in a mouse model of retinitis pigmentosa, Cell Death Differ 22 (2015) 476-487.
54. Y. Munemasa, Y. Kitaoka, Autophagy in axonal degeneration in glaucomatous optic neuropathy, Prog Retin Eye Res 47 (2015) 1-18.
55. T. Wei, Q. Kang, B. Ma, S. Gao, X. Li, Y. Liu, Activation of autophagy and paraptosis in retinal ganglion cells after retinal ischemia and reperfusion injury in rats, Exp Ther Med 9 (2015) 476-482.

ACCEPTED MANUSCRIPT

56. I. Piano, E. Novelli, L. Della Santina, E. Strettoi, L. Cervetto, C. Gargini, Involvement of Autophagic Pathway in the Progression of Retinal Degeneration in a Mouse Model of Diabetes, Front Cell Neurosci 10 (2016)
57. S.G. Kim, G.R. Buel, J. Blenis, Nutrient regulation of the mTOR complex 1 signaling pathway, Mol Cells 35 (2013) 463-473.
58. Y. Liu, R. Wang, Z. Zhao, W. Dong, X. Zhang, X. Chen, L. Ma, Short-term caloric restriction exerts neuroprotective effects following mild traumatic brain injury by promoting autophagy and inhibiting astrocyte activation, Behav Brain Res 331 (2017) 135-142.
59. W. Dong, R. Wang, L.N. Ma, B.L. Xu, J.S. Zhang, Z.W. Zhao, Y.L. Wang, et al., Autophagy involving age-related cognitive behavior and hippocampus injury is modulated by different caloric intake in mice, Int J Clin Exp Med 8 (2015) 11843-11853.
60. D. Cervia, G. Casini, The Neuropeptide Systems and their Potential Role in the Treatment of Mammalian Retinal Ischemia: A Developing Story, Curr Neuropharmacol 11 (2013) 95-101.
61. H. Sun, S. Zou, K.A. Candiotti, Y. Peng, Q. Zhang, W. Xiao, Y. Wen, et al., Octreotide Attenuates Acute Kidney Injury after Hepatic Ischemia and Reperfusion by Enhancing Autophagy, Sci Rep 7 (2017) 42701.
62. S. Muller, S. Brun, F. Rene, J. de Seze, J.P. Loeffler, H. Jeltsch-David, Autophagy in neuroinflammatory diseases, Autoimmun Rev 29 (2017) 30139-30138.
63. A. Markovinovic, R. Cimbro, T. Ljutic, J. Kriz, B. Rogelj, I. Munitic, Optineurin in amyotrophic lateral sclerosis: Multifunctional adaptor protein at the crossroads of different neuroprotective mechanisms, Prog Neurobiol 154 (2017) 1-20.
64. R.A. Frake, T. Ricketts, F.M. Menzies, D.C. Rubinsztein, Autophagy and neurodegeneration, J Clin Invest 125 (2015) 65-74.
65. R.A. Nixon, J. Wegiel, A. Kumar, W.H. Yu, C. Peterhoff, A. Cataldo, A.M. Cuervo, Extensive involvement of autophagy in Alzheimer disease: an immuno-electron microscopy study, J Neuropathol Exp Neurol 64 (2005) 113-122.
66. J. Wei, H. Jiang, H. Gao, G. Wang, Blocking Mammalian Target of Rapamycin (mTOR) Attenuates HIF-1alpha Pathways Engaged-Vascular Endothelial Growth Factor (VEGF) in Diabetic Retinopathy, Cell Physiol Biochem 40 (2016) 1570-1577.
67. B. Liu, L. Faia, M. Hu, R.B. Nussenblatt, Pro-angiogenic effect of IFNgamma is dependent on the PI3K/mTOR/translational pathway in human retinal pigmented epithelial cells, Mol Vis 16 (2010) 184-193.
68. J. Zhang, Y. Bai, L. Huang, Y. Qi, Q. Zhang, S. Li, Y. Wu, et al., Protective effect of autophagy on human retinal pigment epithelial cells against lipofuscin fluorophore A2E: implications for age-related macular degeneration, Cell Death Dis 12 (2015) 330.
69. N.N. Liu, N. Zhao, N. Cai, Suppression of the proliferation of hypoxia-Induced retinal pigment epithelial cell by rapamycin through the /mTOR/HIF-1alpha/VEGF/ signaling, IUBMB Life 67 (2015) 446-452.
70. A. Stahl, L. Paschek, G. Martin, N.J. Gross, N. Feltgen, L.L. Hansen, H.T. Agostini, Rapamycin reduces VEGF expression in retinal pigment epithelium (RPE) and inhibits RPE-induced sprouting angiogenesis in vitro, FEBS Lett 582 (2008) 3097-3102.
71. C.S. Lee, E.Y. Choi, S.C. Lee, H.J. Koh, J.H. Lee, J.H. Chung, Resveratrol Inhibits Hypoxia-Induced Vascular Endothelial Growth Factor Expression and Pathological Neovascularization, Yonsei Med J 56 (2015) 1678-1685.
72. R. Liegl, S. Koenig, J. Siedlecki, C. Haritoglou, A. Kampik, M. Kernt, Temsirolimus inhibits proliferation and migration in retinal pigment epithelial and endothelial cells via mTOR inhibition and decreases VEGF and PDGF expression, PLoS One 9 (2014)
73. C.H. Lin, C.H. Li, P.L. Liao, L.S. Tse, W.K. Huang, H.W. Cheng, Y.W. Cheng, Silibinin inhibits VEGF secretion and age-related macular degeneration in a hypoxia-dependent manner through the PI-3 kinase/Akt/mTOR pathway, Br J Pharmacol 168 (2013) 920-931.

ACCEPTED MANUSCRIPT

74. H.Y. Park, J.H. Kim, C.K. Park, Activation of autophagy induces retinal ganglion cell death in a chronic hypertensive glaucoma model, Cell Death Dis 5 (2012) 26.
75. V. Connaughton. Glutamate and Glutamate Receptors in the Vertebrate Retina. In H. Kolb, E. Fernandez, and R. Nelson (eds.), Webvision: The Organization of the Retina and Visual System, Salt Lake City (UT), 2005 (updated 2007).
76. R.E. Marc, R.F. Murry, S.F. Basinger, Pattern recognition of amino acid signatures in retinal neurons, J Neurosci 15 (1995) 5106-5129.

ACCEPTED MANUSCRIPT

Figure Legends

Fig. 1. Representative western blotting images of LC3 (A), p62 (B) and phosphorylated S6 (pS6) (C) expression in control explants (UT), in HG-treated explants (HG), and in HG-treated explants in the presence of OCT (HG+OCT). GAPDH (A and B) and total S6 (C) were used as internal standards. Lower panels: densitometric analysis of LC3-II, p62 and pS6 levels relative to their respective standard. Results are expressed as fold change of UT (n = 6-13 explants, each originating from a different retina). *$p < 0.05$ relative to UT; §$p < 0.001$ relative to HG.

Fig. 1. Representative confocal images showing the pattern of LC3 immunofluorescence (green) in control explants (A), in HG-treated explants (B), and in HG-treated explants in the presence of OCT (C). Insets are higher-power and higher-contrast images of the boxed areas of the corresponding color. Retinal layers are visualized with DAPI counterstain (blue). Scale bar, 20 µm (10 µm for the insets). D, quantitative analysis of immunofluorescence levels. Results are expressed as fold change of control (n = 4 explants, each originating from a different retina). *$p < 0.001$ relative to control; §$p < 0.001$ relative to HG. GCL, ganglion cell layer; INL, inner nuclear layer; IPL, inner plexiform layer; ONL, outer nuclear layer; OPL, outer plexiform layer.

Fig. 2. Representative confocal images showing the pattern of p62 immunofluorescence (green) in control explants (A), in HG-treated explants (B), and in HG-treated explants in the presence of OCT (C). Insets are higher-power and higher-contrast images of the boxed areas. Retinal layers are visualized with DAPI counterstain (blue). Scale bar, 20 µm (10 µm for the insets). n = 4 explants, each originating from a different retina. Abbreviations as in figure 2.

Fig. 4. Double-label immunofluorescence using antibodies directed to LC3 (A, D, G, and J) in conjunction with antibodies directed to MAb115A10 (B), GAT-1 (E), Dab1 (H) or ß-tubulin III (K). C, F, I, and L are overlay images. Panels A-C show that the brightly LC3 immunolabeled profiles

ACCEPTED MANUSCRIPT

are distinct from MAb115A10 immunostained bipolar cells, although fainter LC3 immunolabeling can be seen within the somata of these cells (inset in C). Panels D-F show that only a few of the LC3 immunolabeled profiles are also GAT-1 immunostained (arrows). Panels G-I show that most LC3 immunolabeled cells in the proximal INL are also Dab1 immunostained (arrows), while several Dab1 immunoreactive somata result devoid of LC3 immunoreactivity (arrowheads). Finally, panels J-L show that virtually all LC3 immunolabeled profiles in the GCL are also ß-tubulin III immunostained, and vice-versa; the inset in L is a higher-power and higher-contrast image of the boxed area. Representative confocal images from n = 4 explants, each originating from a different retina. Scale bar, 20 µm in A-I, 37 µm in J-L, 10 µm in the insets. Abbreviations as in figure 2.

Fig. 5. (A) Representative western blotting images of LC3 expression in HG-treated explants (HG), in HG-treated explants in the presence of CQ (HG+CQ), and in HG-treated explants in the presence of both CQ and OCT (HG+CQ+OCT). GAPDH was used as internal standard. Lower panel: densitometric analysis of LC3-II levels relative to GAPDH. Results are expressed as fold change of HG (n = 4-5 explants, each originating from a different retina). *$p < 0.05$ relative to HG; §$p < 0.0001$ relative to HG, HG+CQ and HG+OCT. (B) LC3-II net flux determined by subtracting the densitometric value of LC3-II amount in HG samples non-treated with CQ from the corresponding sample treated with CQ, both in the absence and in the presence of OCT. Results are expressed as percentage of HG. *$p < 0.05$ relative to HG.

Fig. 6. Representative confocal images showing the pattern of LC3 immunofluorescence (green) in HG-treated explants (A), in HG-treated explants in the presence of CQ (B), and in HG-treated explants in the presence of both CQ and OCT (C). Insets are higher-power and higher-contrast images of the boxed areas of the corresponding color. Retinal layers are visualized with DAPI counterstain (blue). Scale bar, 20 µm (10 µm for the insets). D, quantitative analysis of immunofluorescence levels. Results are expressed as fold change of HG (n = 4 explants, each

ACCEPTED MANUSCRIPT

originating from a different retina). ; *p < 0.01, **p < 0.001 relative to HG; §p < 0.001 relative to HG+CQ. Abbreviations as in figure 2.

Fig. 7. Representative western blotting images of cleaved (active) caspase-3 in: untreated control explants (UT), CQ-treated explants (CQ), HG-treated explants (HG), HG-treated explants incubated in the presence of OCT (HG+OCT) and HG-treated explants in the presence of both CQ and OCT (HG+CQ+OCT). GAPDH was used as internal standard. Lower panel: densitometric analysis of cleaved caspase-3 levels relative to GAPDH. Results are expressed as fold change of UT (n = 7-10 explants, each originating from a different retina). *p < 0.05 relative to UT; §p < 0.05 relative to HG; #p < 0.0001 relative to HG+CQ and CQ; &p < 0.0001 relative to HG+OCT.

Fig. 8. Retinal sections immunostained either with LC3 (A, D, and G) (green) or with cleaved (active) caspase-3 (B, E, and H) (red) antibodies. DAPI counterstain (C, F, and I) (blue) is shown to visualize the retinal layers. The sections were from untreated control explants (A-C), from HG-treated explants (D-F), and from HG-treated explants incubated in the presence of OCT (G-I). Representative confocal images from n = 4 explants, each originating from a different retina. Scale bar, 20 μm. Abbreviations as in figure 2.

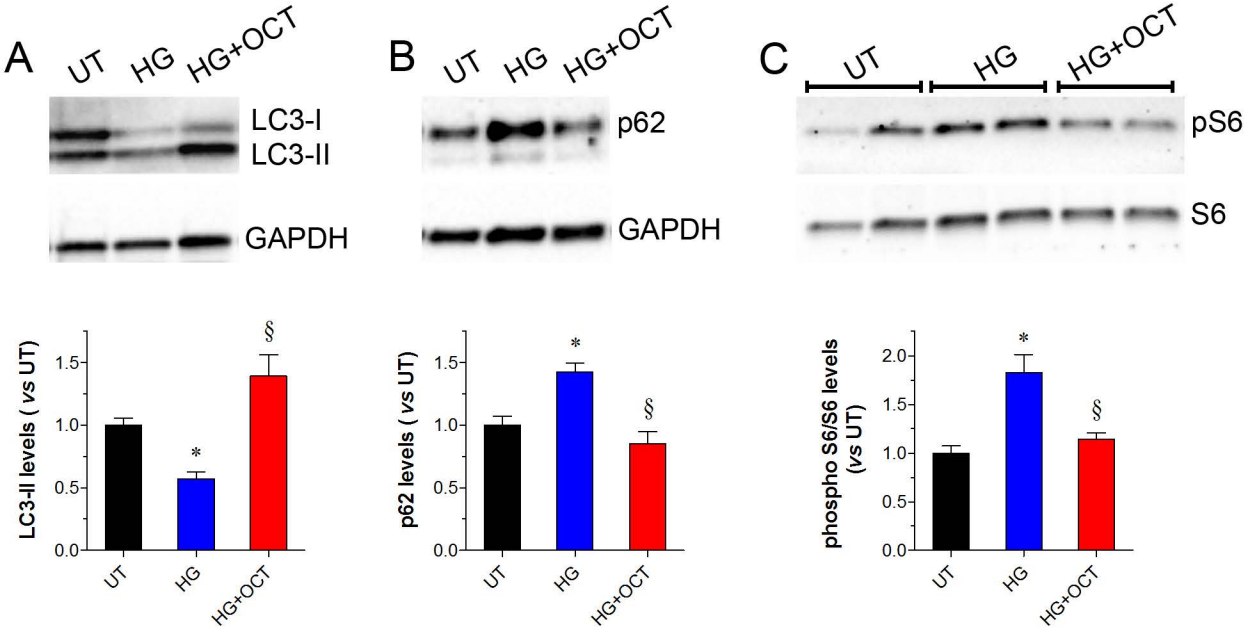
A
UT
HG
HG+OCT
LC3-I
LC3-II
GAPDH
B
UT
HG
HG+OCT
p62
GAPDH
C
UT
HG
HG+OCT
pS6
S6
LC3-II levels (vs UT)
p62 levels (vs UT)
phospho S6/S6 levels (vs UT)
*
§
0.0
0.5
1.0
1.5
2.0
UT
HG
HG+OCT

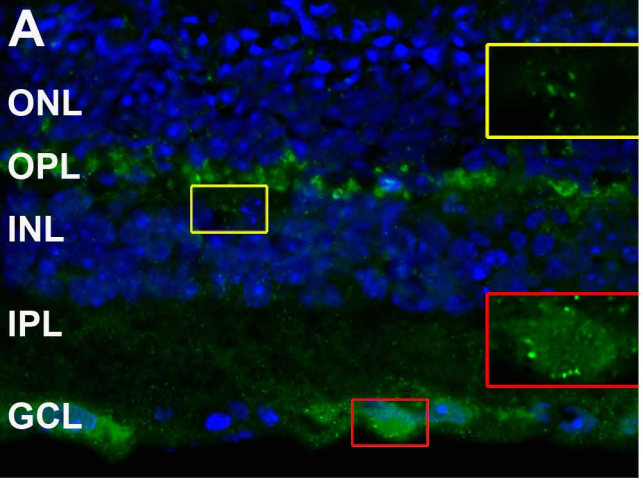
A
ONL
OPL
INL
IPL
GCL

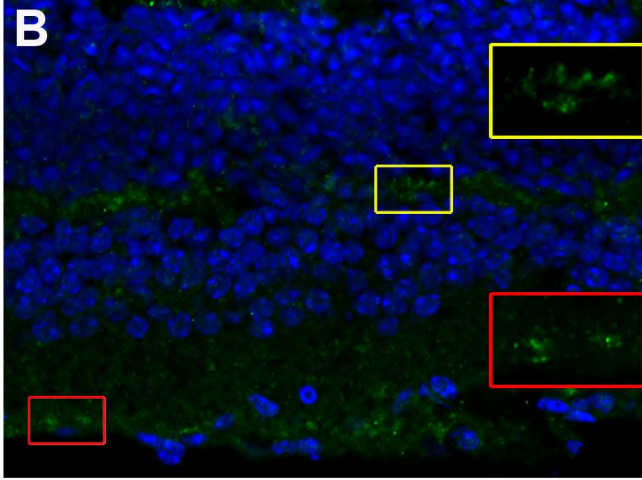
B

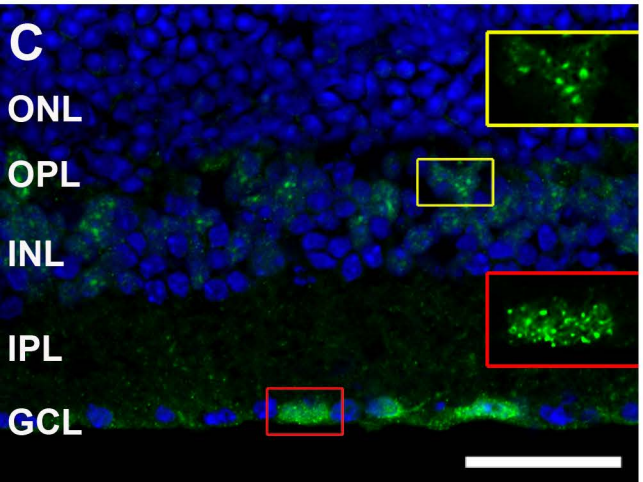
C
ONL
OPL
INL
IPL
GCL

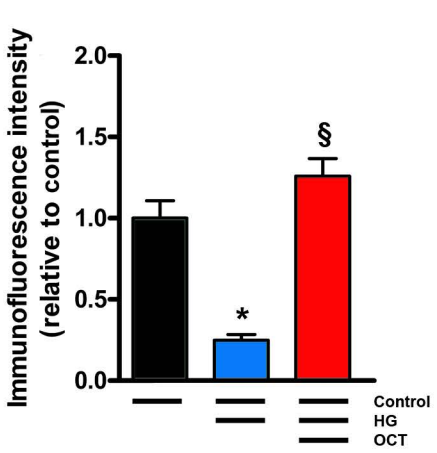
D
Immunofluorescence intensity
(relative to control)
2.0
1.5
1.0
0.5
0.0
*
§
Control
HG
OCT

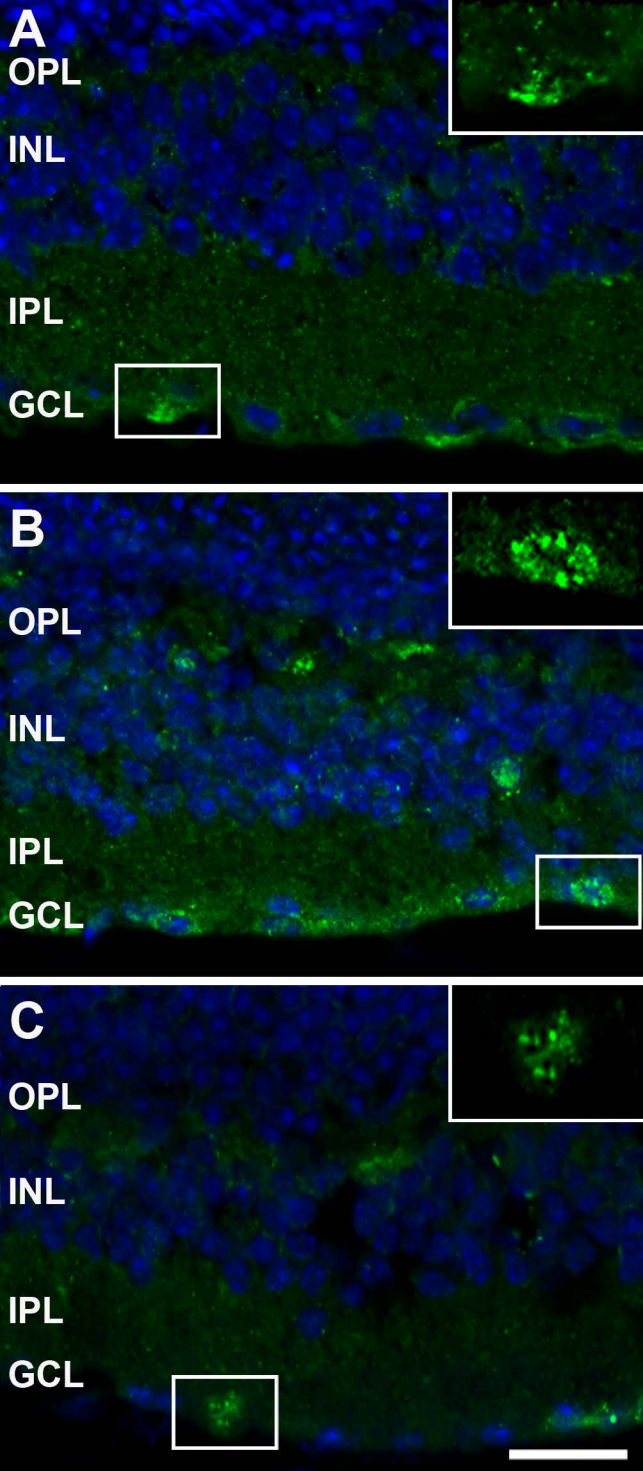
A
OPL
INL
IPL
GCL
B
OPL
INL
IPL
GCL
C
OPL
INL
IPL
GCL

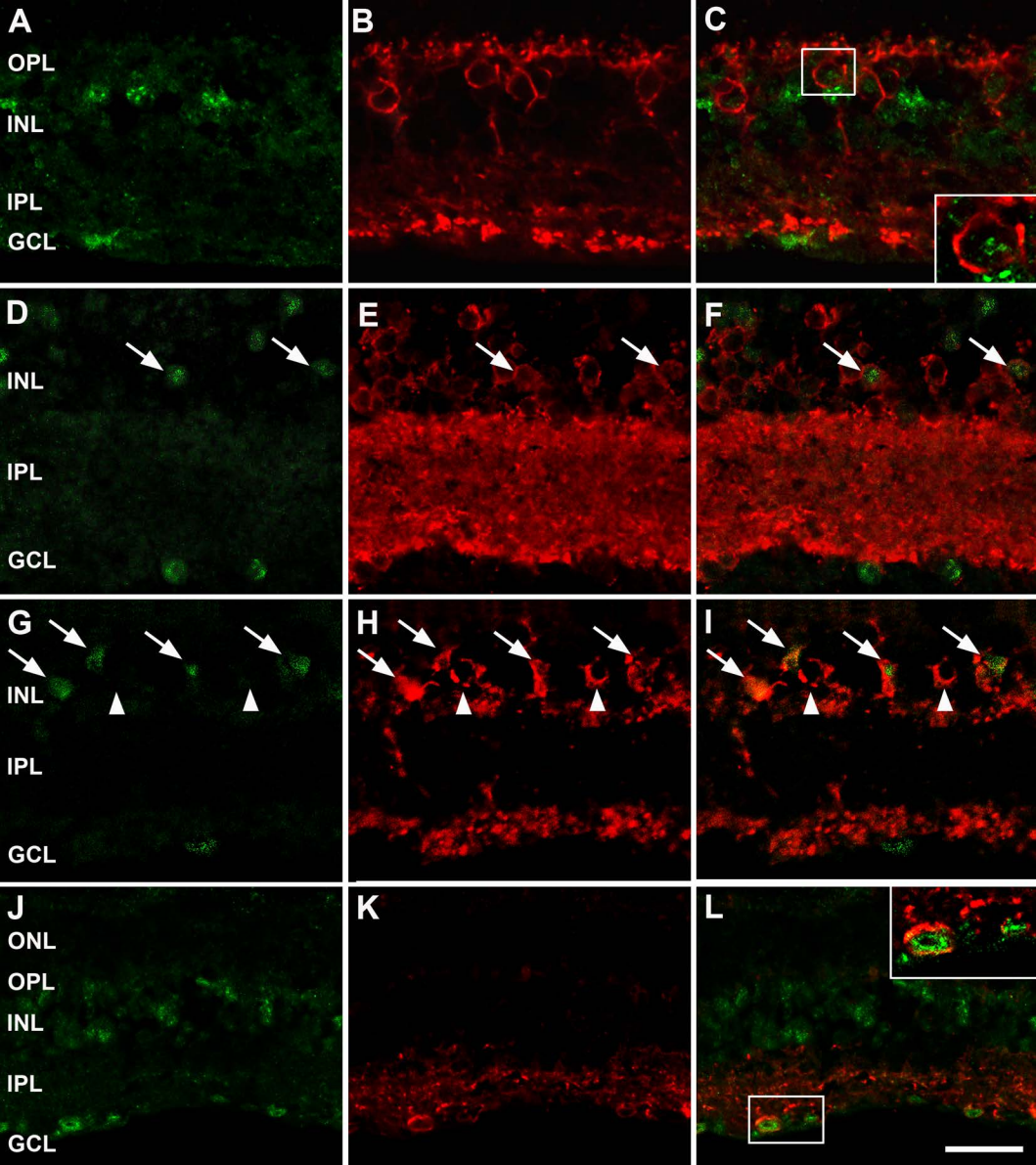
A
OPL
INL
IPL
GCL
B
C
D
INL
IPL
GCL
E
F
G
INL
IPL
GCL
H
I
J
ONL
OPL
INL
IPL
GCL
K
L

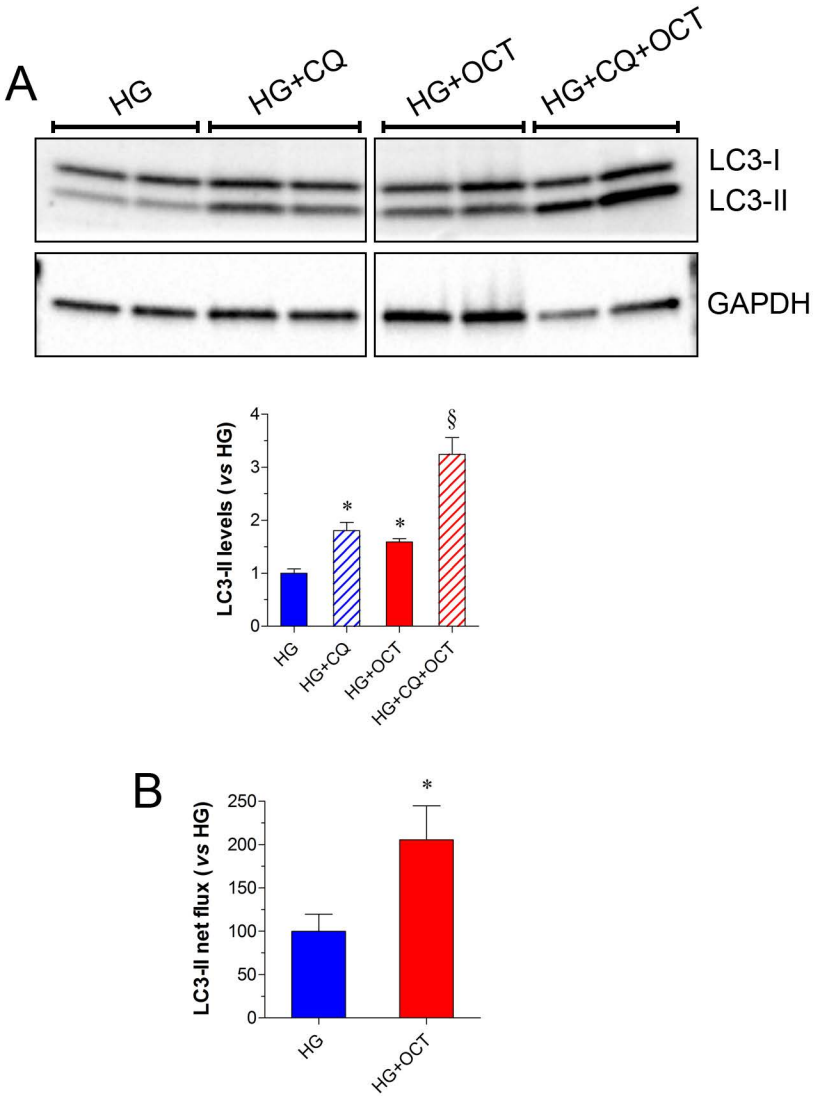
A
HG
HG+CQ
HG+OCT
HG+CQ+OCT
LC3-I
LC3-II
GAPDH
LC3-II levels (vs HG)
0
1
2
3
4
*
*
§
HG
HG+CQ
HG+OCT
HG+CQ+OCT
B
LC3-II net flux (vs HG)
0
50
100
150
200
250
*
HG
HG+OCT

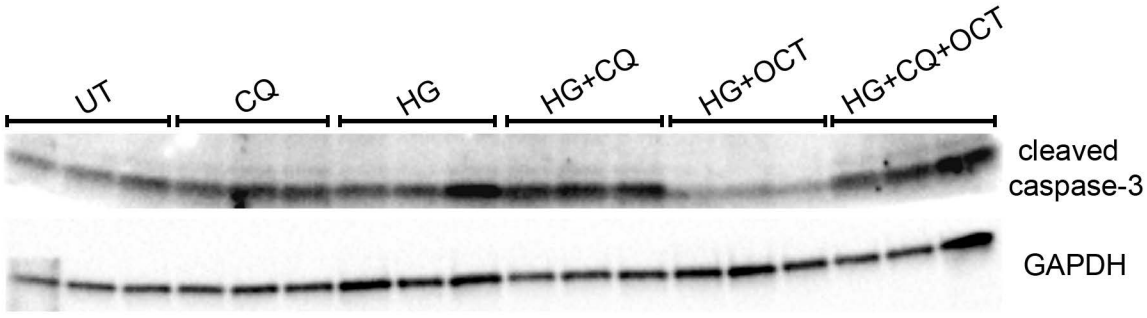
UT
CQ
HG
HG+CQ
HG+OCT
HG+CQ+OCT
cleaved caspase-3
GAPDH

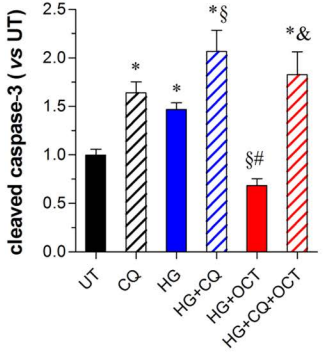
cleaved caspase-3 (vs UT)
2.5
2.0
1.5
1.0
0.5
0.0
*
*
*§
§#
*&
UT
CQ
HG
HG+CQ
HG+OCT
HG+CQ+OCT

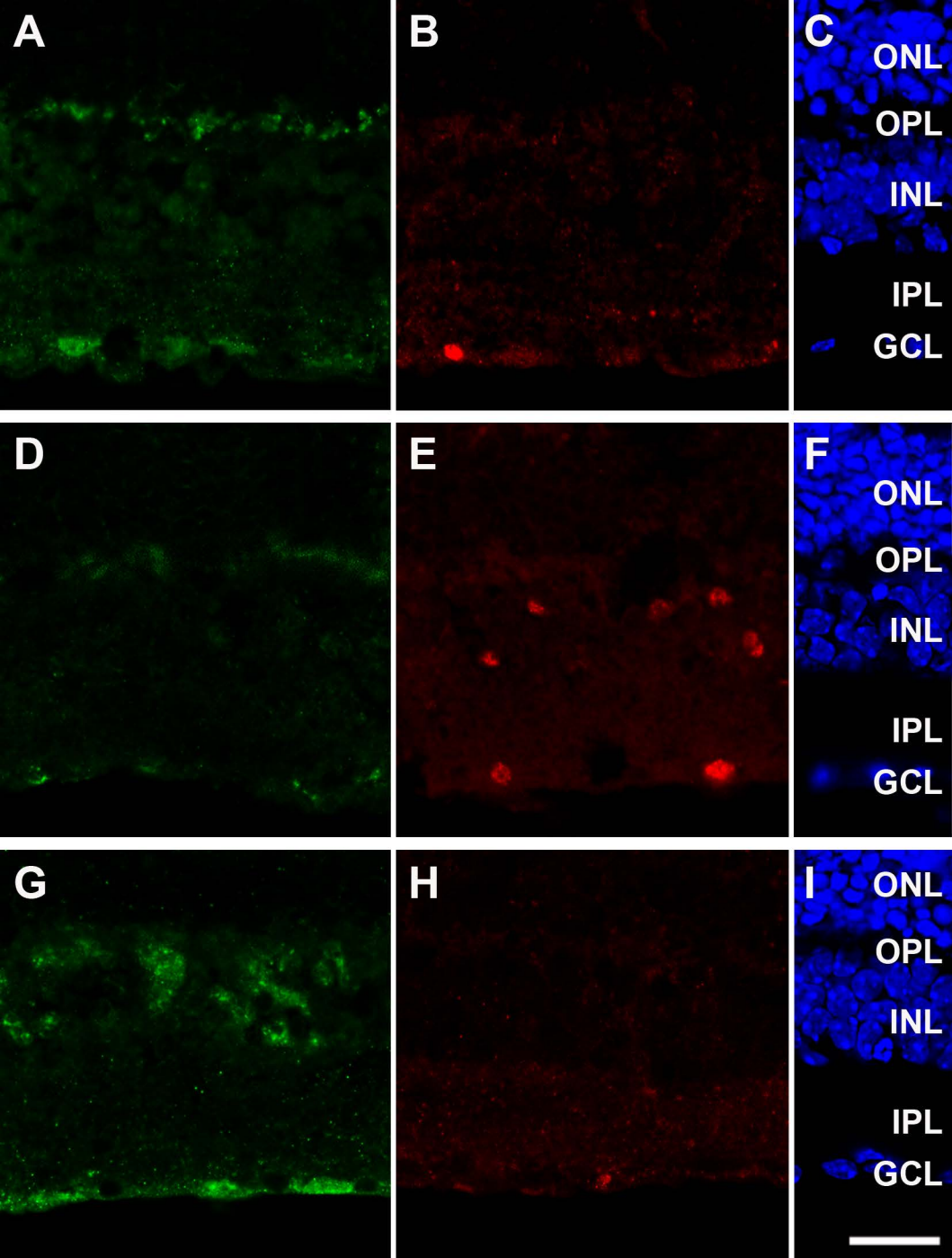
A
B
C
ONL
OPL
INL
IPL
GCL
D
E
F
ONL
OPL
INL
IPL
GCL
G
H
I
ONL
OPL
INL
IPL
GCL